Suppressor of cytokine signaling 3-derived peptide as a therapeutic for inflammatory and oxidative stress-induced damage to the retina

Chulbul M. Ahmed,[1] Anil P. Patel,[1] Howard M. Johnson,[2] Cristhian J. Ildefonso,[3] Alfred S. Lewin[1]

[1]Department of Molecular Genetics and Microbiology, University of Florida Gainesville, FL; [2]Department of Microbiology and Cell Science, University of Florida Gainesville, FL; [3]Department of Ophthalmology, University of Florida Gainesville, FL; Correspondence to: Department of Molecular Genetics and Microbiology P.O. Box 100266 University of Florida Gainesville, FL 32610; Phone: (352) 273-5935; FAX: (352) 273-8905; email: lewin@ufl.edu

Purpose: Inflammation and oxidative stress contribute to age-related macular degeneration (AMD) and other retinal diseases. We tested a cell-penetrating peptide from the kinase inhibitory region of an intracellular checkpoint inhibitor suppressor of cytokine signaling 3 (R9-SOCS3-KIR) peptide for its ability to blunt the inflammatory or oxidative pathways leading to AMD.

Methods: We used anaphylatoxin C5a to mimic the effect of activated complement, lipopolysaccharide (LPS), and tumor necrosis factor alpha (TNFα) to stimulate inflammation and paraquat to induce mitochondrial oxidative stress. We used a human retinal pigment epithelium (RPE) cell line (ARPE-19) as proliferating cells and a mouse macrophage cell line (J774A.1) to follow cell propagation using microscopy or cell titer assays. We evaluated inflammatory pathways by monitoring the nuclear translocation of NF-κB p65 and mitogen-activated protein kinase p38. Quantitative reverse transcription polymerase chain reaction (qRT-PCR) and Western blot were used to evaluate the induction of inflammatory markers. In differentiated ARPE-19 monolayers, we evaluated the integrity of tight junction proteins through microscopy and the measurement of transepithelial electrical resistance (TEER). We used intraperitoneal injection of sodium iodate in mice to test the ability of R9-SOC3-KIR to prevent RPE and retinal injury, as assessed by fundoscopy, optical coherence tomography, and histology.

Results: R9-SOCS3-KIR treatment suppressed C5a-induced nuclear translocation of the NF-kB activation domain p65 in undifferentiated ARPE-19 cells. TNF-mediated damage to tight junction proteins in RPE, and the loss of TEER was prevented in the presence of R9-SOCS3-KIR. Treatment with the R9-SOCS3-KIR peptide blocked the C5a-induced expression of inflammatory genes. The R9-SOCS3-KIR treatment also blocked the LPS-induced expression of interleukin-6, MCP1, cyclooxygenase 2, and interleukin-1 beta. R9-SOCS3-KIR prevented paraquat-mediated cell death and enhanced the levels of antioxidant effectors. Daily eye drop treatment with R9-SOCS3-KIR protected against retinal injury caused by i.p. administration of sodium iodate.

Conclusions: R9-SOCS3-KIR blocks the induction of inflammatory signaling in cell culture and reduces retinal damage in a widely used RPE/retinal oxidative injury model. As this peptide can be administered through corneal instillation, this treatment may offer a convenient way to slow down the progression of ocular diseases arising from inflammation and chronic oxidative stress.

Age-related macular degeneration (AMD) is a leading cause of loss of central vision, affecting nearly 50 million people worldwide, and with the aging population, its incidence will increase in the coming years [1]. Inflammation and oxidative stress are major drivers of the onset and propagation of AMD [2]. The accumulation of oxidized lipoproteins and free radicals in retinal and choroidal tissue, leading to chronic oxidative injury, results in a full-blown inflammatory process, which enhances oxidative injury and thus self-perpetuates this vicious cycle. An important characteristic of AMD is the presence of drusen, which are extracellular proteolipid deposits located between the retinal pigment epithelium (RPE) and Bruch's membrane [3]. Drusen contain the byproducts of local inflammation, complement activation, and oxidized lipid and carbohydrate waste products [4]. Continuous injury to the RPE layer results in a compromised blood–retinal barrier that allows cytokines and chemokines to enter and activate choroidal dendritic cells. Advanced AMD presents as a "dry" form of the disease, known as geographic atrophy, and leads to progressive and irreversible loss of central vision. The "wet" form of the disease, characterized by choroidal neovascularization (CNV), occurs in about 10% of AMD patients and may cause a sudden loss of central vision [4–7]. CNV may respond to antivascular endothelial growth factor (VEGF) treatments delivered through intravitreal injection [8]. Blocking the VEGF pathway has drawbacks [9] and does not prevent ongoing inflammatory damage.

An overactive complement system is a critical mediator of AMD, diabetic retinopathy, and Stargardt disease [4,10,11].

Anaphylatoxins C5a and C3a, produced by the alternative complement pathway, are detected in the drusen and serum of patients with AMD [10,12–14]. The Y402H variant of complement factor H, a serum protein that normally tempers the alternative complement pathway, increases the progression of AMD [15,16]. The United States Food and Drug Administration has approved two complement inhibitors for treating AMD: pegcetacoplan, a complement C3 inhibitor, and avacincaptad pegol, a C5 inhibitor. Both treatments require repeated intravitreal injections.

A set of intracellular checkpoint protein inhibitors known as suppressors of cytokine signaling (SOCS) suppresses the expression of cytokines [17–19]. Among these, SOCS1 and SOCS3 control Janus kinase/signal transducer and activator of transcription proteins (JAK/STAT) and toll-like receptor (TLR) signaling and are important regulators of the extent and duration of immune responses. SOCS1 and SOCS3 are present in most somatic cells and allow cross-talk between somatic cells and immune cells, suggesting the interconnected nature of their regulatory roles. Despite their importance in modulating inflammation, SOCS proteins have received less attention than the program death 1 cell protein (PD-1) and its ligand PD-1L, and cytokine T lymphocyte antigen 4 and its receptor [20]. Evidence suggests that STAT1 mediates SOCS1 signaling, while SOCS3 acts through STAT3 [18,19,21–23]. Most cytokines and growth factors leading to AMD act through STAT3 [24,25]; thus, we argue that the use of a SOCS3 mimetic may be beneficial in suppressing inflammation, leading to AMD. For SOCS1, we have shown that the kinase inhibitory region of the protein (KIR) by itself is sufficient to achieve inhibition of the target kinases [26,27]. The native protein contains a SOCS box responsible for the proteasomal degradation of SOCS1. As the KIR region of the peptide lacks a SOCS box, it is likely to sustain more cycles of inhibition of its target. In fact, it was shown for the SOCS3 protein that while the endogenous protein had a half-life of 0.7 h, a cell-penetrating peptide of SOCS3 without the SOCS box had a half-life of 29 h [28]. In this study, we presented data with a cell-penetrating peptide containing the KIR of SOCS3 (abbreviated as R9-SOCS3-KIR). We established the protective role of R9-SOCS3-KIR in response to activated complement, lipopolysaccharide (LPS), tumor necrosis factor alpha (TNFα,) and oxidative damage in cell culture models. In a mouse model of acute oxidative stress induced by sodium iodate injection, eye drop instillation of R9-SOCS3-KIR prevented retinal injury.

METHODS

Cell culture: ARPE-19 cells (CRL-2302) were obtained from ATCC (Manassas, VA) and grown in a 1:1 mixture of Dulbecco's Modified Eagle Medium (DMEM) and Hams F12 nutrient mixture (Sigma-Aldrich, St. Louis, MO) with 10% fetal bovine serum (FBS) and 1% each of penicillin and streptomycin in a humidified incubator at 37 °C and 5% CO_2. Where indicated, the cells were grown in 1% FBS (low serum) or serum-free media. The murine macrophage cell line, J774A.1 (ATCC, TIB-67), was grown in DMEM with 10% FBS and 1% each of penicillin and streptomycin. Identity was certified by ATCC. The cells were frozen immediately after their first passage and were passaged no more than three times for use in these experiments.

Peptide synthesis: The following peptides were chemically synthesized to 95% purity using GenScript (Piscataway, NJ). The peptide R9-SOCS3-KIR, with the sequence RRRRRRRRRLRLKTFSSKSEYQLVV, consisted of residues 20–35 from the KIR of SOCS3. The nine arginine residues on the N-terminus were included to allow penetration across biologic membranes. An inactive control peptide with a scrambled version of the KIR sequence with the sequence RRRRRRRRRKSQYVRLSVLFEKTSL was used as a control. The peptides were dissolved in phosphate-buffered saline (PBS) for use.

NF-kB promoter assay: The plasmid pNF-kB-Luc has an NF-kB promoter linked to firefly luciferase. A plasmid that constitutively expresses Renilla luciferase from the thymidine kinase promoter (pRL-TK-Luc) was purchased from Promega (Madison, WI). pRL-TK-Luc serves as an internal control to test the efficiency of transfection. ARPE-19 cells were seeded at 80% confluency in 12-well plates and grown overnight. Cells in triplicate were placed in a serum-free medium and treated with R9-SOCS3-KIR or the control peptide (both at 20 μM) for 1 h, followed by treatment with C5a peptide (Abcam) at 50 ng/ml for 4 h. The cells were transfected using 2 μg of pNF-kB-Luc and 10 ng of pRL-TK-Luc per well using Lipofectamine (Invitrogen, San Diego, CA) for 24 h. The dual luciferase assay kit was obtained from Promega, and the firefly and Renilla luciferase activities were measured in cell lysates using a luminometer, following the manufacturer's instructions.

Immunohistochemistry: The ARPE-19 or J774A.1 cells were seeded at 80% confluency in eight-well chamber slides and grown overnight. They were placed in a serum-free medium and treated with the indicated concentrations of R9-SOCS3-KIR or the control peptide for 1 h, followed by 50 ng/ml of C5a peptide (Abcam) for 0.5 h. The cells were washed and fixed with 4% paraformaldehyde for 30 min at room

temperature and washed with PBS, followed by permeabilization with 1% Triton X-100 in PBS for 30 min at room temperature. The cells were then blocked in 10% normal goat serum in PBS containing 0.5% Triton X-100, followed by washing in 0.2% Triton X-100 in PBS (wash buffer). Rabbit polyclonal antibody for the NF-kB p65 subunit (Cell Signaling Technology) at 1:200 dilution was added and incubated overnight at 4 °C, followed by washing four times with the wash buffer. Cy3-conjugated anti-rabbit secondary antibody (Invitrogen, 1:300 dilution) was added and incubated for 0.5 h, followed by washing four times. The slides were co-stained with 4′,6′-diamidino-2-phenylindole (DAPI). After the mounting media was added, the cells were coverslipped, and imaged in a Keyence BZ-X700 fluorescence microscope. In other experiments, *Escherichia coli* LPS or paraquat (both from Sigma-Aldrich) was used at the concentrations indicated. Antibodies to phospho-STAT3 and phospho-p38 were obtained from Cell Signaling. Alexa-488-conjugated secondary antibody was obtained from Thermo Fisher. To obtain differentiated ARPE-19 cells, the cells were grown in 1% FBS-containing media, with twice-weekly changes of media for four weeks until the cells acquired a cuboidal morphology. They were treated with R9-SOCS3-KIR or the control peptide at 20 µM for 3 h, followed by incubation with C5a (50 ng/ml) or TNFα (10 ng/ml) for 48 h. Afterward, the processing of the cells was similar to that described above. The cells were then incubated overnight with an antibody to ZO-1 (Invitrogen), followed by a Cy3-conjugated secondary antibody. The steps for further processing were similar to those described earlier [26].

Measurement of transepithelial electrical resistance (TEER): ARPE-19 cells were seeded in 24-well Transwell inserts (Griener Bio-one, 0.4 µm size) in 1% FBS-containing media for ARPE-19 cells, with twice-weekly changes in media for four weeks until the cells began to look cuboidal. The cells were treated with 20 µM R9-SOCS3-KIR or the control peptide for 3 h, followed by treatment with C5a peptide (50 ng/ml) or TNFα (10 ng/ml) for 48 h. TEER was measured using a voltohmmeter (EVOM2, World Precision Instruments), following the manufacturer's instructions. The inserts were removed one at a time and placed in the EVOM-2 chamber filled with serum-free medium to take the TEER measurements. The value of a blank Transwell filter was subtracted from each sample to obtain the net TEER.

Enzyme-linked immunosorbent assay (ELISA): The J774A.1 cells were seeded in 96-well plates at 80% confluency and grown overnight. They were placed in a 1% FBS-containing medium and treated with 20 µM R9-SOCS3-KIR or the control peptide for 1 h, followed by treatment with C5a

peptide (50 ng/ml) and incubation overnight. The supernatants were harvested and used in triplicate to measure the concentration of VEGF-A through ELISA using a kit from PeproTech (Cranbury, NJ). In another experiment, following the peptide treatment of the J774A.1 cells, LPS (1 µg/ml) was added, and the cells were incubated overnight. Supernatants were harvested and used in triplicate to quantitate interleukin-1 beta (IL-1β) using the ELISA kit from PeproTech.

Measurement of released nitric oxide: The J774A.1 cells were seeded at 80% confluence in 96-well plates and grown overnight. They were placed in 1% FBS-containing medium and treated with increasing concentrations of R9-SOCS3-KIR or 30 µM of the control peptide for 1 h, followed by the addition of LPS (1 µg/ml) and grown overnight. The supernatants were harvested and used in triplicate to measure nitric oxide concentration using Greiss reagent (Alexis Biochemicals, Plymouth Meeting, PA), following the manufacturer's protocol. A standard curve was generated using sodium nitrite as a substrate to determine the concentration in the experimental samples.

RNA extraction and qPCR: The ARPE-19 or J774A.1 cells were seeded at 80% confluency in 12-well plates and grown overnight. ARPE-19 cells were transferred to serum-free media and treated with 20 µM R9-SOCS3-KIR for 1 h, followed by treatment with C5a (50 ng/ml) for 4 h. The J774A.1 cells were similarly placed in serum-free media and treated with LPS (1 µg/ml) in one experiment and with paraquat (300 µg/ml) in another for 4 h. The cells were washed with PBS. Total RNA was extracted using TRIzol reagent (Invitrogen) and purified using the DirectZol RNA kit from Zymo Research (Irvine, CA). The i-Script kit from Bio-Rad (Hercules, CA) was used to generate cDNA. Quantitative polymerase chain reaction (qPCR) was performed using a kit from Bio-Rad, following the conditions described previously [26]. The sequence of primers used is provided in **Table 1**. The primers were synthesized by Eurofins (Louisville, KY). For the retinas obtained from mouse eyes, we used a similar procedure. As an internal control, β-actin primers were used, and the relative RNA concentrations were determined using the $^{\Delta\Delta}$Ct method [29].

Western blot analysis: The J774A.1 cells were seeded at 80% confluence in six-well plates and grown overnight. They were transferred to a 1% FBS-containing medium and treated with R9-SOCS3-KIR or the control peptide for 1 h, followed by treatment with LPS (1 µg/ml) and incubation overnight. From each sample, 20 µg of proteins were loaded on a 12% polyacrylamide gel separated by electrophoresis and then transferred to a polyvinylidene difluoride membrane using an iBlot system (Thermo Fisher, Waltham, MA). The membrane

TABLE 1. NUCLEOTIDE SEQUENCE OF PCR PRIMERS USED FOR QPCR.

Gene	Primer (5'-3')	
Human primers		
IL-1β -F	F: CTCGCCAGTGAAATGATGGCT	R: GTCGGAGATTCGTAGCTGGAT
IL-6-F	F: CTTCTCCACAAGCGCCTTC	R: CAGGCAACACCAGGAGCA
IL17A-F	F: ATTGGTGTCACTGCTACTGCT	R: AGGTGAGGTGGATCGGTTGT
MCP-1-F	F: CTCATAGCAGCCACCTTCATTC	R: TCACAGCTTCTTTGGGACACTT
HO-1-F	F: CCAGCGGGCCACAACAAAGT	R: GCCTTCAGTGCCCACGGTAAGG
NQO-1-F	F: AAAGGACCCTTCCGGAGTAA	R: CCATCCTTCCAGGATTTGAA
SOD-2-F	F: GTGTGGGAGCACGCTTACTA	R: AGAGCTTAACATACTCAGCATAACG
Nrf2-F	F: GTCCCAGCAGGACATGGATTT	R: GCTGAATTGGGAGAAATTCACCTG
NQO-1-F	F: AAAGGACCCTTCCGGAGTAA	R: CCATCCTTCCAGGATTTGAA
b-actin-F	F: AGCGAGCATCCCCCAAAG TT	R: GGGCACGAAGGCTCATCATT
Murine primers		
IL-1β -F	F: GCAGCAGCACATCAACAAGAGC	R: TCGGAGCCTGTAGTGCAGTTG
IL-6-F	F: GTTGCCTTCTTGGGACTGATG	R: GCACAACTCTTTTCTCATTCCACG
MCP-1-F	F: TCTGGGCCTGCTGTTCACAGTT	R: CCTCTCTCTTGAGCTTGGTGAC
COX-2-F	F: GAAGTCTTTGGTCTGGTGCCTG	R: GAAACTGTTTGAAGCTGTACTCCTGG
HO-1-F	F: AGCCCCACCAAGTTCAAACA	R: GCAGTATCTTGCACCAGGCT
GSTM-1-F	F: GGGATACTGGAACGTCCGC	R: GCTCTGGGTGATCTTGTGTGA
NQO-1-F	F: CGACAACGGTCCTTTCCAGA	R: CCAGACGGTTTCCAGACGTT
Catalase-F	F: CGCAATCCTACACCATGTCG	R: AGTATCCAAAAGCACCTGCTCC
b-actin-F	F: CGAGCACAGCTTCTTTGCA	R: TTCCCACCATCACACCCTGG

was soaked in a blocking buffer from Li-Cor Biosciences (Lincoln, NE) for 1 h, followed by incubation with antibodies to cyclooxygenase 2 (COX-2) and α-tubulin (the source of these reagents is provided in Table 2) as an internal control overnight. The membrane was rinsed four times with PBS containing 0.1% Tween-20. The appropriate infrared (IR) dye-conjugated secondary antibodies (Li-Cor Biosciences; 1:5000 dilution in a blocking buffer) were added for 0.5 h. The membrane was washed with the blocking buffer four times and scanned using an Odyssey IR imaging system (Li-Cor Biosystems). The experiment was repeated two more times using independent cell samples. Using the ImageJ system (NIH), the relative intensities of COX-2 and α-tubulin were calculated and plotted next to the first Western blot image. A one-way analysis of variance (ANOVA), followed by Tukey's test for multiple comparisons, was used to determine the statistical differences in the relative intensities of bands under different treatments.

Sodium iodate-induced mouse model of oxidative stress: The University of Florida Institutional Animal Care and Use Committee approved all procedures involving mice. Animal experiments were conducted in accordance with the Statement for the Use of Animals in Ophthalmic and Vision Research of

the Association for Research in Vision and Ophthalmology. C57BL/6 mice (BomTac; n = 20; 10 male and 10 female) were divided into two groups: one for treatment with R9-SOCS3-KIR and the other with the control peptide. These mice had been tested to ensure that they did not carry the *Pde6β*rd1 or the *Crb1*rd8 mutations. The peptides were instilled in both eyes at 15 μg/eye in 2 μl once per day. Pre-treatment with these peptides started on day −1 and continued daily until day 3. On day 1, mice were injected i.p. with 25 mg/kg of sodium iodate, as described previously [30]. On day 3, fundoscopy and optical coherence tomography (OCT) were performed. At the end of this, the mice were humanely sacrificed, and their retinas were harvested for RNA extraction and used for cDNA synthesis, followed by qPCR as described above.

Retinal imaging and cell counting: Digital fundoscopy and spectral-domain OCT were performed, as described previously [26]. To measure the thickness of the outer nuclear layer (ONL), we recorded four measurements (temporal, nasal, superior, and inferior) at a distance of 0.35 mm from the optic nerve head of each eye. The ONL thickness of both eyes was averaged, and the mean thickness for each group was calculated.

TABLE 2. SOURCE OF REAGENTS USED.		
Reagent	**Source**	**Cat number**
Anti-p65 antibody	Cell Signaling Tech	8242
Anti-pSTAT3 antibody	Cell Signaling Tech	9145
Anti-p-p38 antibody	Cell Signaling Tech	4511
Anti-ZO-1 antibody	Invitrogen	40-2200
Anti-COX-2 antibody	Cell Signaling Tech	12282
Anti-α-Tubulin antibody	AbCam	Ab7291
Cy-3 conjugated 2° ab	ThermoFisher	A-10520
Alexxa-488 conjugated 2°ab	ThermoFisher	A-11008
VEGF ELISA ABTS kit	PeproTech	900-K99
IL-1β ELISA ABTS kit	PeproTech	900-M47

ImageJ software was used to count the cells infiltrating the vitreous. The area corresponding to the vitreous was marked, and reflective spots corresponding to the infiltrating cells were converted into binary images. To determine the number of cells in each area, we used the count particle function of ImageJ, as described previously [26]. The number of infiltrating cells in both eyes of each mouse was averaged, and the number of infiltrating cells in the R9-SOCS3-KIR or control peptide groups was compared.

Histopathology: On day 3, after sodium iodate administration, mice were humanely sacrificed. The eyes were dissected and placed in 4% paraformaldehyde overnight at 4 °C. The samples were washed in PBS, dehydrated using a graded series of alcohol solutions, and embedded in paraffin. Sectioning was performed through the cornea–optic nerve axis at a thickness of 12 μm. Eight step sections were collected on different slides and stained with hematoxylin and eosin, and the slides were prepared for microscopy.

Statistical analysis: The experiments from the cell culture are presented as average ± standard deviation. We used a two-tailed Student's *t*-test to compare the mean transcript levels for unpaired data. The results for the mouse studies are presented as the average ± standard deviation. For the experiments that involved comparing more than two samples, we used a one-way ANOVA and Tukey's test to identify the statistical significance using GraphPad Prism 8.2.1 software (San Diego, CA). A p-value or adjusted p-value of less than 0.05 was considered statistically significant.

RESULTS

R9-SOCS3-KIR dampens the response to activated complement: The activation of the alternate pathway of the complement system is a major contributor to the inflammatory response in AMD [4,7]. Given this critical role of activated complement, we tested the effect of anaphylatoxin C5a on RPE-like cells to follow the effects on the pathways leading to inflammatory damage. After binding to the receptor, C5a acts through the NF-κB promoter [31,32]. Cross-talk of C5a with the TLR-4 system also causes activation of the NF-κB pathway [33]. We used a dual luciferase assay to analyze the NF-κB activation in RPE-like cells. Undifferentiated ARPE-19 cells were pre-treated with 20 μM R9-SOCS3-KIR or its control peptide for 1 h, followed by treatment with the C5a peptide at 50 ng/ml for 4 h. Treatment was followed by co-transfection with a firefly luciferase-linked NF-kB promoter plasmid and a plasmid expressing Renilla luciferase under the control of the thymidine kinase promoter as an internal control. The C5a and R9-SOCS3-KIR peptides remained in the culture for 24 h before relative luciferase units were determined using a dual luciferase reporter kit (Promega, Madison, WI). C5a treatment caused a ninefold induction of the NF-κB promoter activity (Figure 1A). In the presence of R9-SOCS3-KIR, induction was only 1.9-fold. Treatment with C5a in the presence of the control peptide led to a 6.5-fold increase in activation of NF-kB promoter activity, indicating that the blockade of induction depended on the peptide's sequence.

We analyzed the nuclear translocation of the p65 subunit of NF-κB in response to complement treatment as an independent assay of NF-κB activation (Figure 1B). Treatment with C5a resulted in the nuclear translocation of p65 in most cells, indicating the activation of the NF-κB pathway. The cells pre-treated with R9-SOCS3-KIR followed by C5a did not exhibit a nuclear accumulation of p65. At the same time, the negative control peptide did not affect the translocation of NF-κB, indicating the specificity of the action of R9-SOCS3-KIR.

Complement activation can lead to increased cell permeability and damage to the tight junctions between RPE cells, and increased levels of TNFα may contribute to choroidal neovascularization and stimulate epithelial-to-mesenchymal transition in the RPE [34,35]. Therefore, we tested the effects of C5a and TNFα on RPE cells. To determine whether

R9-SOCS3-KIR could protect the RPE monolayer, ARPE-19 cells were grown in low-serum media for four weeks until the cells had differentiated and acquired a cobblestone-like morphology. These cells were pre-treated with R9-SOCS3-KIR or the control peptide (20 μM) for 3 h and treated with C5a peptide (50 ng/ml) for 48 h. At the end of the treatment
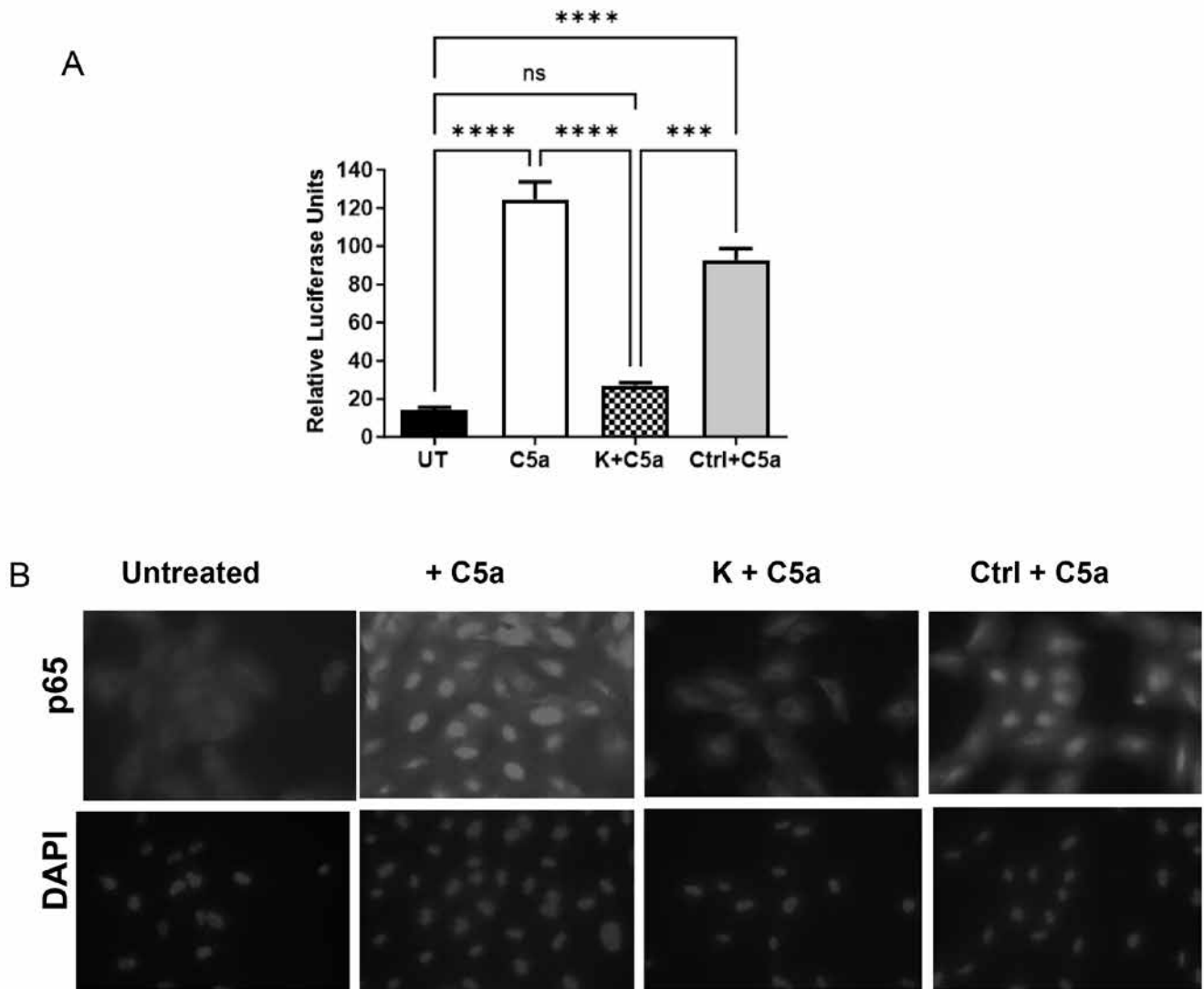
Figure 1. R9-SOCS3-KIR suppressed the C5a-mediated induction of the NF-kB promoter. **A**: The ARPE-19 cells in a serum-free medium were treated with R9-SOCS3-KIR or the control peptide (20 μM) for 1 h, followed by treatment with C5a (50 ng/ml) for 4 h. The cells were then co-transfected with a mixture of plasmids with NF-kB promoter-driven firefly luciferase and another plasmid with thymidine kinase-driven Renilla luciferase as an internal control and grown for 24 h in a 1% FBS-containing medium. The cell lysates were harvested to measure the relative luciferase units using a dual luciferase kit from Promega. ****, p<0.0001. Error bars indicate the standard deviation. Abbreviations: K, R9-SOCS3-KIR; Ctrl, R9-SOCS3-KIR-scrambled peptide; UT, untreated. **B.** R9-SOCS3-KIR suppressed the C5a-induced nuclear translocation of the NF-κB subunit p65. The ARPE-19 cells were grown overnight in eight-well plates, placed in a serum-free medium, and treated with R9-SOCS3-KIR or its control peptide at 20 μM for 1 h, followed by the addition of C5a (50 ng/ml) for 30 min. The cells were stained with an antibody to p65, Cy3-conjugated secondary antibody, and DAPI and then imaged in a fluorescence microscope using the same exposure time and light intensity. Abbreviations: K, R9-SOCS3-KIR; Ctrl, R9-SOCS3-KIR-scrambled peptide; UT, untreated. Scale bar: 50 μm.

with C5a, the cells were permeabilized and treated with an antibody to ZO-1 (zonula occludens 1), followed by incubation with a Cy3-conjugated secondary antibody, washed, fixed, and imaged with fluorescence microscopy (Figure 2A,B). The untreated cells showed a continuous distribution of the tight junction protein along the neighboring cells, indicating the integrity of the monolayer, as expected for the differentiated RPE cells. Treatment with either the C5a peptide or TNFα resulted in an irregular distribution of the

tight junction protein, with marked disruptions between cells, as expected of cells in stress [36]. The presence of R9-SOCS3-KIR prevented the loss of ZO-1 along the cell membranes. The control peptide did not affect the loss of ZO-1 caused by C5a or TNFα.

The loss of tight junction proteins results in a decrease in TEER [37]. We measured TEER in the differentiated ARPE-19 cells with a voltohmmeter. The C5a treatment caused a 72% decrease in TEER compared with the untreated
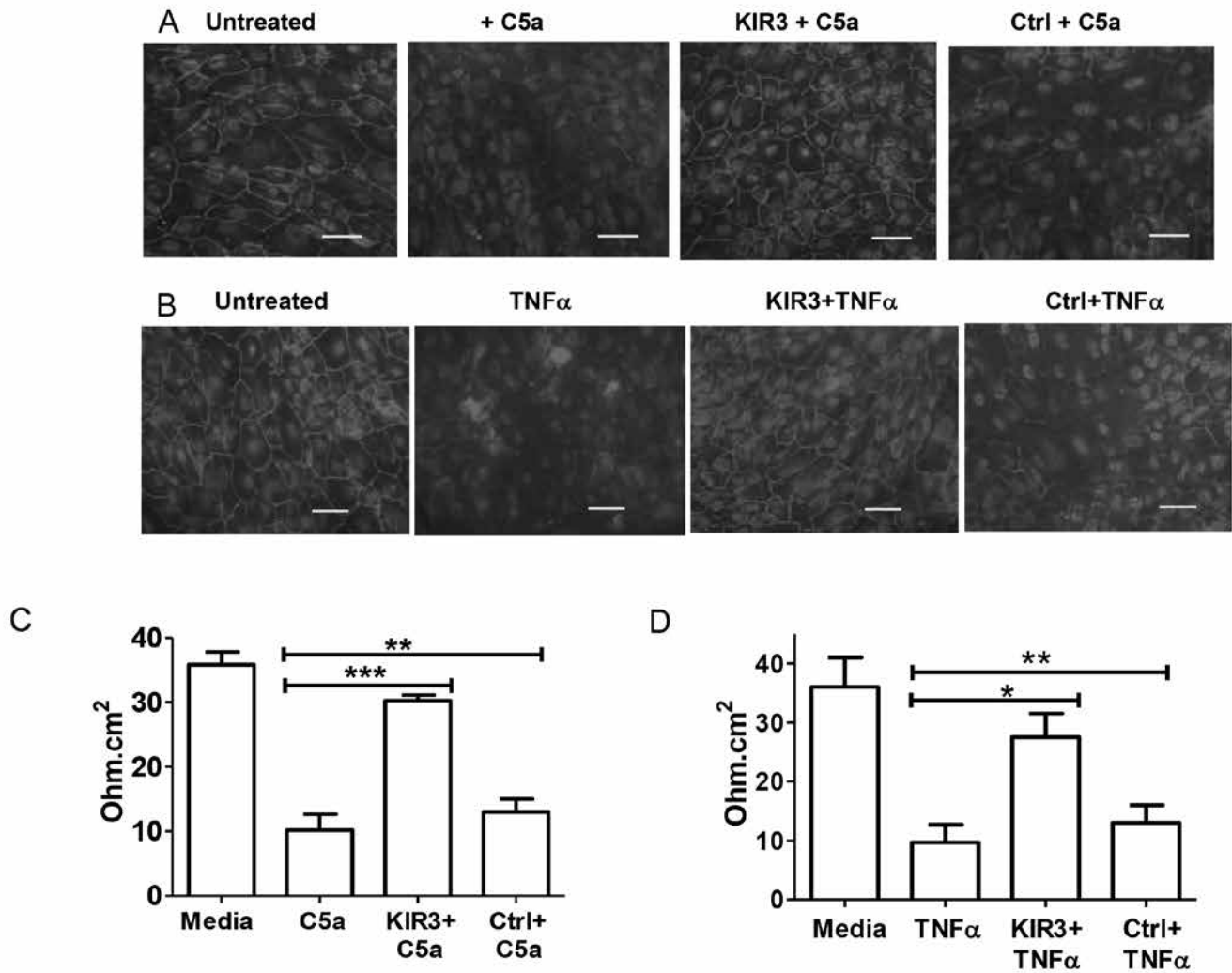

Figure 2. R9-SOCS3-KIR prevented the loss of tight junction proteins and transepithelial electrical resistance (TEER) caused by C5a and TNFα. The ARPE-19 cells were grown in 24-well Transwell plates for four weeks in low serum until they attained a cobblestone morphology. They were pre-treated with R9-SOCS3-KIR or its control peptide (both at 20 µM) for 2 h, followed by treatment with (**A**) C5a (50 ng/ml) or (**B**) TNFα (10 ng/ml) for 48 h. The cells were permeabilized and treated with an antibody to ZO-1, incubated with a Cy3-conjugated secondary antibody, washed, fixed, and imaged using a Keyence fluorescence microscope. Scale bar: 50 µm. The TEER was measured in individual wells in triplicate using an EVOM2 voltohmmeter. **C**: TEER measurements in response to C5a ± R9-SOCS3-KIR. **D**: TEER measurements in response to TNFα ± R9-SOCS3-KIR. Abbrev: KIR-3, R9-SOCS3-KIR, Ctrl, scrambled R9-SOCS3-KIR peptide. One-way ANOVA (ANOVA), followed by Tukey's multiple comparisons, was used to test significance. *, $p < 0.05$; ***, $p < 0.001$, ****, $p < 0.0001$. Abbreviations: KIR-3, R9-SOCS3-KIR; Ctrl, scrambled R9-SOCS-3 KIR peptide.
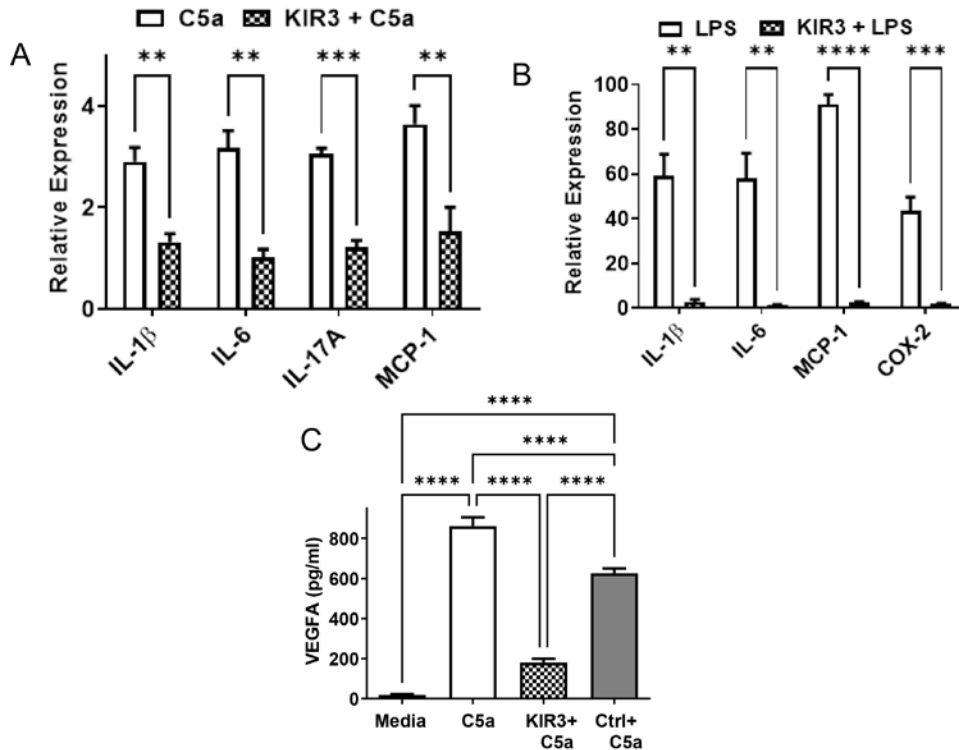
Figure 3. C5a and LPS-induced inflammatory mediators were suppressed in the presence of R9-SOCS3-KIR. **A**: The ARPE-19 cells were seeded in six-well plates and grown overnight. They were placed in serum-free media and treated with or without R9-SOCS3-KIR (20 µM) for 1 h, followed by treatment with C5a peptide (50 ng/ml) for 4 h. Quantitative RT-PCR was conducted using the primers for the target genes indicated, and β-actin primers served as the internal control. The results represent the average of biologic triplicates, and the error bars indicate the standard deviations. **B**: The anti-inflammatory effects of R9-SOCS3-KIR were observed in LPS-treated J774A.1 cells. The mouse macrophage, J774A.1 cells, were grown overnight in 12-well plates. They were placed in serum-free media and treated with R9-SOCS3-KIR (20 µM) for 1 h, followed by the addition of LPS (1 µg/ml) for 4 h. Quantitative RT-PCR was performed using primers for the target genes indicated, and β-actin primers served as the internal control. The bars represent the average of the triplicates ± standard deviation. For each comparison, statistical significance was assessed using the Student's *t*-test. **, $p < 0.01$; ***, $p < 0.001$; ****, $p < 0.0001$. **C.** J774A.1 cells in 1% FBS-containing media were treated with R9-SOCS3-KIR or the control peptide (at 20 µM) for 1 h, followed by treatment with C5a (50 ng/ml), and incubated overnight. The supernatants were harvested and used to quantify VEGF-A using an ELISA kit from PeproTech. ****, $p < 0.0001$, as determined by one-way ANOVA.

cells (Figure 2C). In the presence of R9-SOCS3-KIR, the loss of TEER caused by C5a was only 16%, while the control peptide showed a 70% decrease in TEER, indicating the protective role of R9-SOCS3-KIR in maintaining the integrity of tight junction proteins in the presence of C5a. Treating the ARPE-19 cells with TNFα decreased TEER by 70%, while TEER decreased by only 20% in the presence of R9-SOCS3-KIR (Figure 2D). In the sample treated with the control peptide, TEER was reduced by 64%, indicating the protective role of R9-SOCS3-KIR in preserving tight junction proteins in response to TNFα.

To test the ability of R9-SOCS3-KIR to suppress the inflammatory markers induced by C5a, we measured the transcript levels of the inflammatory cytokines using quantitative reverse transcription polymerase chain reaction (qRT-PCR; Figure 3A). Treatment with C5a caused a 3–3.5-fold increase in the RNA levels of the cytokines IL-1β, IL-6, and IL-17A and the chemokine MCP-1. However, these levels diminished 2-3-fold when treated with R9-SOCS3-KIR, indicating the immunosuppressive effect of this peptide.

Thus, R9-SOCS3-KIR is a potent inhibitor of C5a toxicity at multiple levels and can dampen its effect.

R9-SOCS3-KIR protects against the inflammatory damage caused by LPS: To evaluate the anti-inflammatory effects of R9-SOCS3-KIR, we used LPS, which activates NF-kB and mitogen-activated protein (MAP) kinase p38 through TLR4 [38,39]. We used a mouse macrophage cell line, J774A.1, as a surrogate for activated mononuclear phagocytes in the retina. In particular, macrophages are known to play a central role in the progression to AMD [40] and diabetic retinopathy [41]. To define the anti-inflammatory actions of R9-SOCS3-KIR in mononuclear phagocytes, we treated the J774A.1 cells with R9-SOCS3-KIR or the control peptide for 1 h, followed by treatment with LPS (1 µg/ml) for 4 h. RNA was extracted from these cells, converted into cDNA, and used as a template for qPCR using the primers for the inflammatory genes indicated (Figure 3B). LPS treatment caused a 60-fold increase in IL-1β and a 57-fold increase in IL-6 transcript levels, which were prevented in the presence of R9-SOCS3-KIR. Although the chemokine MCP-1 transcript increased 90-fold

following LPS treatment, it remained at baseline in the presence of R9-SOCS3-KIR. The transcript for the enzyme COX-2 increased 45-fold but remained at the baseline level in the presence of R9-SOCS3-KIR. Thus, R9-SOCS3-KIR is a potent suppressor of pro-inflammatory gene expression.

R9-SOCS3-KIR reduces the secretion of VEGF-A through mononuclear phagocytes: As invading macrophages exacerbate CNV by elevating VEGF, we tested the effect of R9-SOCS3-KIR on the J774A.1 macrophage cell line. The cells were pre-treated with R9-SOCS3-KIR or the control peptide for 1 h, followed by treatment with C5a (50 ng/ml) and incubation overnight. The cell supernatants were harvested and used for the quantitation of VEGF-A using ELISA. The supernatants of the untreated cells contained 18.4 ± 3.9 pg/ml of VEGF-A, and treatment with C5a resulted in a 47-fold ($p < 0.001$) increase in the VEGF-A level (Figure 3C). Pre-treatment with R9-SOCS3-KIR led to an 80% decrease in the VEGF-A level ($p < 0.001$), while the control peptide treatment resulted in only a 20% decrease in the VEGF-A level ($p < 0.001$), indicating that the reduction in VEGF-A secretion was specific to R9-SOCS3-KIR.

R9-SOCS3-KIR diminishes LPS-induced nuclear translocation of NF-κB: NF-κB mediates the transcription of inflammatory cytokines in response to pro-inflammatory stimuli. To evaluate the effect of the SOC3-KIR peptide on the nuclear translocation of NF-κB and p38 in macrophage cells, we pre-treated the J774A.1 cells in a serum-free medium with R9-SOCS3-KIR or its control (both at 20 μM), followed by the addition of LPS (1 μg/ml) for 30 min. The cells were washed and stained with primary antibodies to p65, which is the active subunit of NF-kB, or with the antibody to phospho-p38 (activated MAP kinase p38). They were washed and stained with fluorescent secondary antibodies and DAPI to visualize the nuclei (Figure 4). LPS treatment caused nuclear translocation of NF-κB (A) and p-p38 (B). However, treatment with the R9-SOCS3-KIR peptide blocked the nuclear translocation of p65 and p38, while the control peptide did not significantly affect either of them. These results suggest that, similar to its effect on ARPE-19 cells (Figure 1B), R9-SOCS3-KIR blocked the nuclear translocation of NF-kB and p38 in macrophage cells, thus explaining its suppression of proinflammatory gene expression (Figure 3).

In addition, we characterized the effect of our peptide on mononuclear phagocyte inflammatory functions. To confirm the protective role of R9-SOCS3-KIR against the inflammatory effect of LPS, we pre-treated the J774A.1 cells with 0, 3, 10, and 30 μg/ml of R9-SOCS3-KIR or 30 μM of the control peptide for 1 h. This was followed by the addition of LPS at 1 μg/ml and incubation overnight. The supernatants

were harvested to quantify nitric oxide using Greiss reagent (Appendix 1). There was a 16% ($p < 0.01$), 45%, and 73% ($p < 0.001$) decrease in the release of nitric oxide in the presence of 3, 10, and 30 μg/ml of R9-SOCS3-KIR, respectively. Conversely, there was only a 4% decrease in nitric oxide in the presence of the control peptide at 30 μg/ml, thus suggesting the dose-dependent inhibition of nitric oxide production in the presence of R9-SOCS3-KIR. We also studied the effect of our peptide on the secretion of proinflammatory cytokines using ELISA. We harvested supernatants from J774A.1 cells that were pre-treated with 20 μg/ml of R9-SOCS3-KIR or its control peptide for 1 h, followed by treatment with LPS at 1 μg/ml overnight. The secretion of IL-1β in these supernatants was quantified using ELISA (Appendix 1). A negligible amount of IL-1β was released from the untreated cells. Treatment with LPS resulted in the secretion of 1,600 pg/ml of IL-1β, which was reduced by 75% in the cells in the presence of R9-SOCS3-KIR. By contrast, the control peptide reduced this secretion by only 20% ($p < 0.0001$ for both), consistent with our qRT-PCR observations (Figure 3). We studied the changes in the protein levels of another marker of macrophage activation [42], COX-2, by performing Western blots with the cell lysates (Supplemental 1C). The J774A.1 cells were pre-treated with R9-SOCS3-KIR or its control peptide at 20 μM for 1 h and treated with LPS at 1 μg/ml for 24 h. The membranes were probed with antibodies to COX-2 and α-tubulin as the internal control. The relative intensities of COX-2 and the internal control α-tubulin were measured using ImageJ (NIH) software (Appendix 1). LPS treatment resulted in a six-fold increase in the synthesis of COX-2, which was reduced to 2.5-fold in the presence of R9-SOCS3-KIR and remained unaffected in the presence of the control peptide, indicating that the R9-SOCS3-KIR peptide caused a reduction in expression of COX-2 protein. Our studies support the hypothesis that R9-SOCS3-KIR-mediated inhibition of STAT3 signaling in mononuclear phagocytes can significantly inhibit their proinflammatory responses.

R9-SOCS3-KIR alleviates the oxidative damage caused by paraquat: As oxidative stress contributes to RPE damage and AMD pathogenesis [43], we measured the effect of SOCS3-KIR on RPE cells treated with paraquat to cause an increase in mitochondrial reactive oxygen species [44]. We treated the ARPE-19 cells with 20 μM of R9-SOCS3-KIR or the control peptide for 1 h, followed by incubation with 300 μM of paraquat for 24 h. The cells were stained with hematoxylin and eosin and viewed in a confocal microscope (Figure 5A). The untreated cells constituted a confluent monolayer, but treatment with paraquat disrupted this layer and left gaping holes. The cells treated simultaneously with R9-SOCS3-KIR were protected from this damage and remained confluent,

while the control peptide did not prevent damage to the cells. We assessed the survival of the ARPE-19 cells using the CellTiter Aqueous reagent (Promega) and identified the absorbance using a plate reader. The cell survival of untreated cells was set to 100%. In the presence of 3, 10, and 30 µg/ml of R9-SOCS3-KIR, we noted a 20%, 50%, and 80% survival of cells, respectively ($p < 0.001$ for all), suggesting a dose-dependent protection against damage caused by paraquat in

these cells (Figure 5B). In the presence of 30 µg/ml of the control peptide, only 20% of the cells survived, suggesting the specificity of the antioxidant effect with the R9-SOCS3-KIR peptide.

To test whether the protection against oxidative damage noted above was associated with the induction of antioxidant factors, we performed qRT-PCR for the effector molecules with protective properties (Figure 6). We noted a 6.5-fold
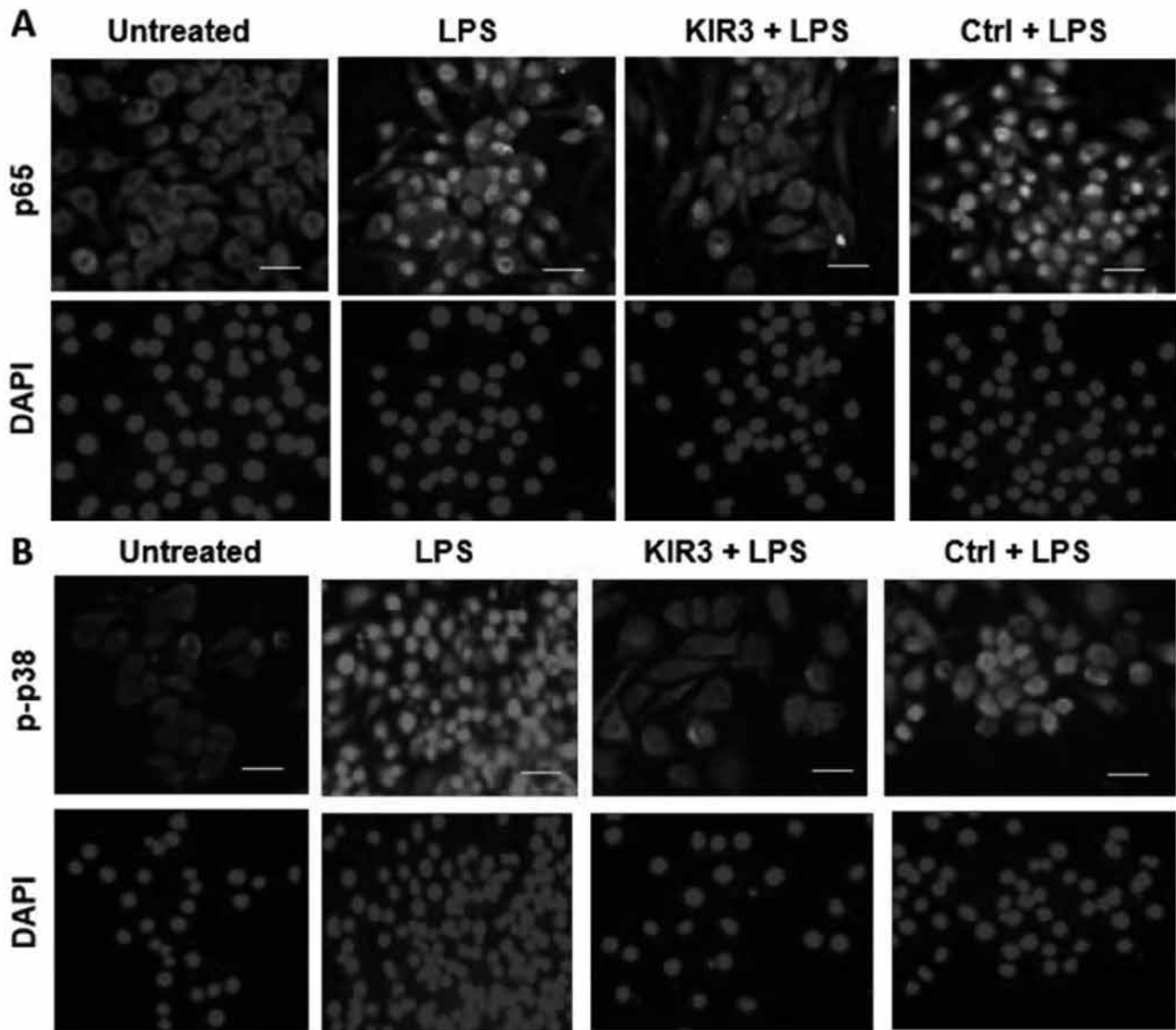

Figure 4. R9-SOCS3-KIR suppressed LPS-induced nuclear translocation of NF-κB and MAP kinase p38 in J774A.1 cells**.** The J774A.1 cells were seeded on an eight-well cell culture slide and grown overnight. The cells were transferred to a serum-free medium and pre-treated with R9-SOCS3-KIR peptide or its control peptide at 20 µM for 1 h, followed by treatment with LPS (1µg/ml) for 30 min. The cells were stained with an antibody to p65, which is the active subunit of NF-κB (**A**), or phosphorylated p38 (p-p38; **B**). Secondary antibodies conjugated to Alexa-488 (**A**, green) or Cy3 red (**B**, red) and DAPI (nuclei, bottom row in A and B) were used and imaged using a fluorescence microscope. Scale bar: 50 µm.
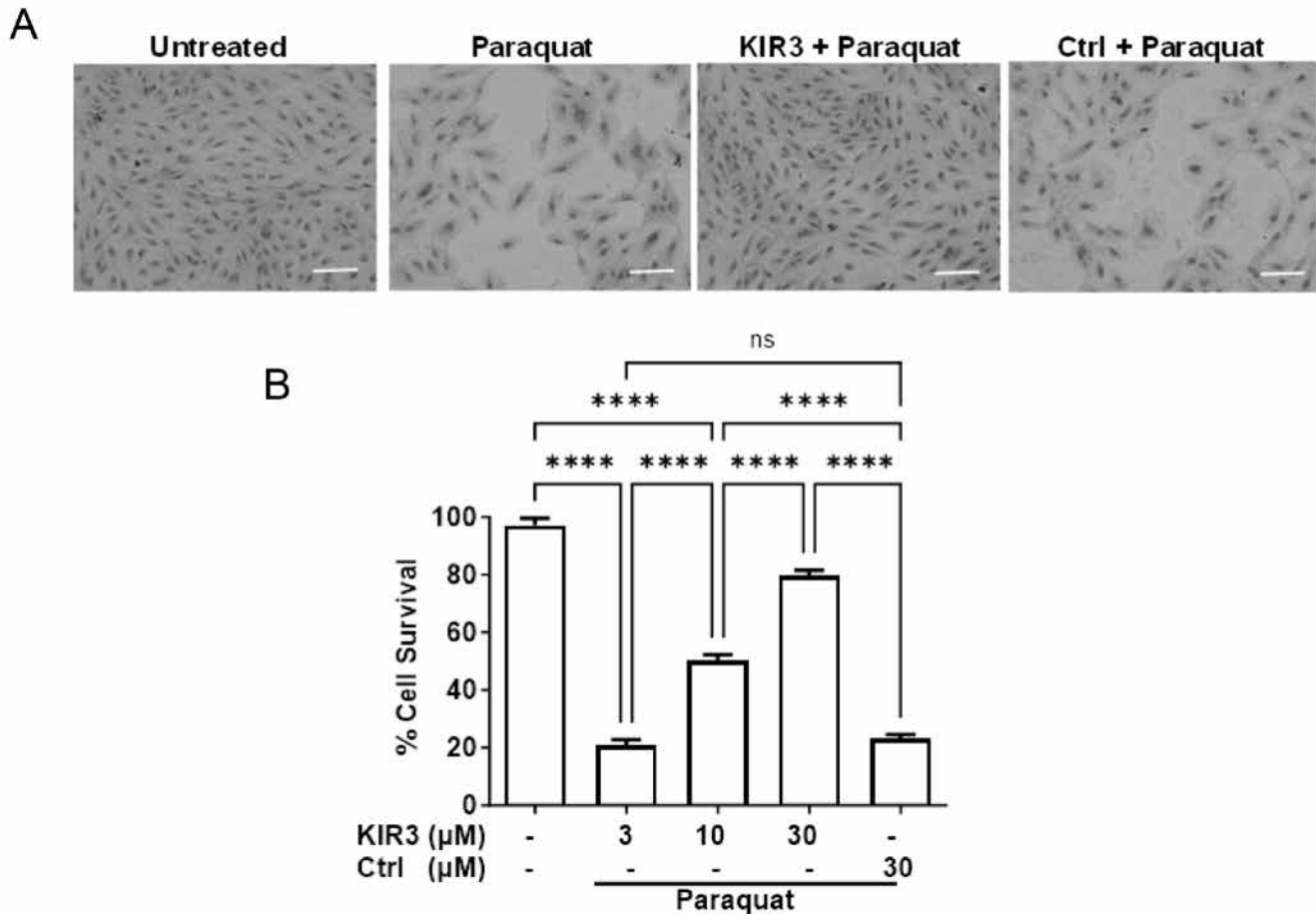
Figure 5. R9-SOCS3-KIR prevented paraquat-mediated oxidative damage to RPE-like cells. **A**: ARPE-19 cells were seeded in eight-well slides and grown overnight before being transferred to a serum-free medium. They were pre-treated with R9-SOCS3-KIR or its control peptide (both at 20 μM) for 1 h and then with paraquat at 300 μM for 48 h. The cells were stained with hematoxylin and eosin and imaged with a confocal microscope. Scale bar: 50 μm. **B**: Cell survival was assessed in cells grown and treated as in (A) using CellTiter Aqueous reagent (Promega), and absorbance was determined using a plate reader. Absorbance in untreated cells was set to 100%. Survival in the other treatments was calculated. One-way ANOVA and Tukey's test for multiple comparisons were used. ****, $p < 0.0001$.

increase in heme oxygenase 1 (HO-1), which was induced 8.7-fold in the presence of R9-SOCS3-KIR. Similarly, the levels of SOD2, Nrf2, and NqO-1 were increased three-fold by paraquat alone and were induced further by 1.5–2-fold in the simultaneous presence of R9-SOCS3-KIR. These genes are regulated by the antioxidant response element and the induction of Nrf2, a transcription factor for antioxidant enzymes, is consistent with the survival of ARPE-19 cells seen in the presence of paraquat.

R9-SOCS3-KIR acts through STAT3 inhibition: There is evidence that SOCS1 inhibits signaling mediated by STAT1, while SOCS3 predominantly inhibits signaling mediated by STAT3 [18,45,46]. SOCS1 binds directly to the kinase domain of specific target JAKs, tyrosine kinases (TYKs), or adaptors, while SOCS3 docks on the gp130 subunit of the IL-6 family

of receptors and subsequently binds to the corresponding kinase domain of specific JAKs.

To demonstrate the effect of R9-SOCS3-KIR acting through STAT3, we treated the ARPE-19 cells with IL-6, which, along with IL-17, is implicated in the progression of dry AMD to geographic atrophy [47] and CNV [48]. The ARPE-19 cells were treated with R9-SOCS3-KIR or the control peptide for 1 h, followed by the addition of IL-6 (50 ng/ml) for 0.5 h. The cells were incubated with an antibody to phospho-STAT3, which is the activated form of STAT3, followed by staining with Alexa-488 conjugated secondary antibody and DAPI. The fixed cells were imaged using a fluorescence microscope (Figure 7). Treatment with IL-6 resulted in the nuclear translocation of pSTAT3 in ARPE-19 cells. This translocation was blocked in the presence of

R9-SOCS3-KIR but not by the vehicle control, thus showing the inhibition of STAT3 signaling by R9-SOCS3-KIR.

Corneal application of R9-SOCS3-KIR protects mouse eyes in the sodium iodate model: Having noted a combination of protective effects on RPE cells and macrophages in the presence of R9-SOCS3-KIR in cell culture studies, we tested its efficacy in protecting eyes from sodium iodate-induced acute oxidative injury. Two groups of C57BL/6 mice (10 males and 10 females) were pre-treated with eye drop administration of R9-SOCS3-KIR or its control peptide (15 µg in 2 µl) in both eyes once a day on days −1 and 0. On day 0, the mice were injected i.p. with 25 mg/kg of sodium iodate. Daily eye drop instillation was continued for three days. On day 3, digital fundoscopy revealed an influx of inflammatory cells and perivascular deposits in the control group, while the R9-SOCS3-KIR-treated mice had less damage (Figure 8A). OCT showed thinning of the ONL and increased cellular infiltration in the control-treated eyes compared with the R9-SOCS3-KIR-treated eyes (Figure 8B). On day 3, the mice (n = 4 in each group) were humanely sacrificed, and their eyes were harvested, fixed, and stained with hematoxylin and eosin (Figure 8C). A larger number of inflammatory cells in the vitreous and retina were observed in the controls, while the R9-SOCS3-KIR-treated eyes had no evident infiltrating cells. Notably, retinal swelling and rosettes (in-foldings) were a common feature of the control eyes and were not found in any of the R9-SOCS3-KIR-treated eyes.

Using ImageJ software, we quantified the number of inflammatory cells in the B-scans from four areas of the posterior chamber from the OCT images. In the control eyes, we noted 60 ± 9 inflammatory cells per image, while the average number of cells in the R9-SOCS3-KIR-treated mice was 12.8 ± 3.4 (n = 18, $p < 0.001$) per image, indicating less inflammation with R9-SOCS3-KIR (Figure 8D). The thickness of the ONL was measured using the autosegmentation software Diver 2.0 of Leica microsystems (Figure 8E). The ONL thickness in the control-treated eyes was 53.1 ± 2.6, while R9-SOS3-KIR-treated eyes had an ONL thickness of 62.2 ± 1.5 ($p < 0.0001$), indicating the protective role of R9-SOCS3-KIR. The ONL measurements showed no significant difference between the male and female mice (data not shown).

We examined the induction of antioxidative genes to investigate the protective effect of R9-SOCS3-KIR in mouse eyes. We harvested the retinas from the control and treated mice (n = 4 from each group) on day 3. RNA was extracted
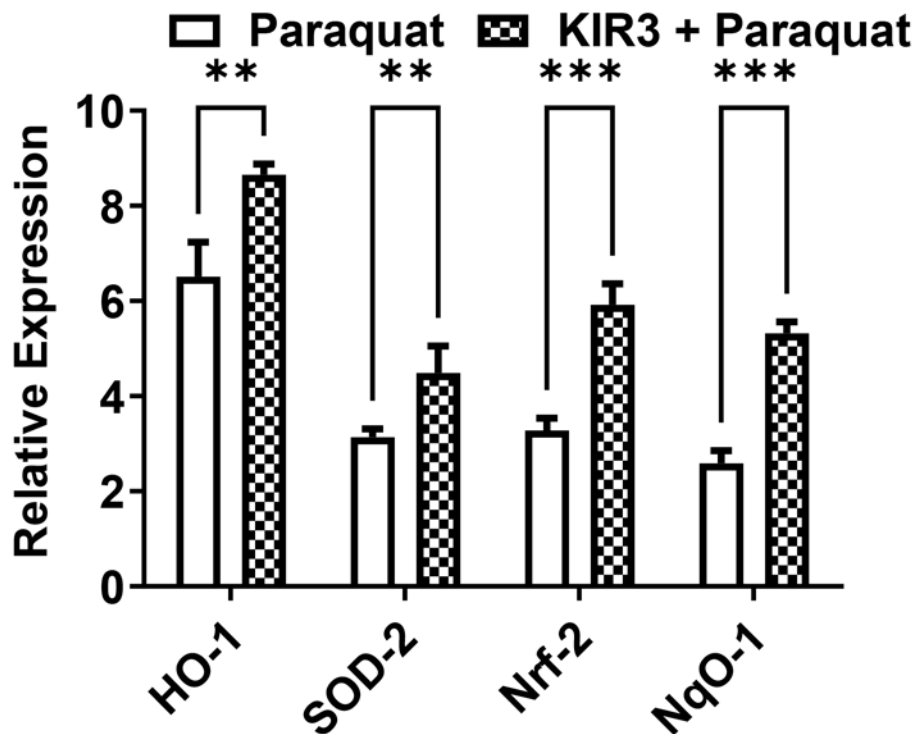

Figure 6. R9-SOCS3-KIR enhanced the antioxidant response in paraquat-treated ARPE-19 cells. ARPE-19 cells were grown overnight in 12-well plates. They were placed in a 1% FBS-containing medium and treated with R9-SOCS3-KIR (20 µM) for 1 h and then with paraquat (300 µM) for 4 h. The cells were washed, and RNA was extracted and used for cDNA synthesis. Quantitative RT-PCR was performed using the primers for the target genes indicated above, and β-actin served as the internal control. The units represent the expression level relative to β-actin. The Student's *t*-test for unpaired data was used to calculate the statistical significance in each set of samples. **, $p < 0.01$, ***, $p < 0.001$. Abbreviations: HO-1, heme oxidase 1; SOD2, superoxide dismutase 2; Nrf2, NFE2-like BZIP transcription factor 2; NQO-1, NAD(P)H quinone dehydrogenase 1.

and used for qRT-PCR (Figure 9). We noted a 3–4-fold increase in HO-1, GSTM-1, NQO-1, and catalase in the R9-SOCS3-KIR-treated eyes compared with the control eyes. The antioxidant effect of these enzymes may have contributed to the protection of the eyes noted above.

DISCUSSION

R9-SOCS3-KIR is a water-soluble, cell-penetrating peptide containing the KIR of the human SOCS3 protein. As this peptide is of human origin, we expect no immune response after delivery to humans. Eye drop administration can restrict its effect to the delivery site and reduce the potential for systemic side effects while allowing patient self-administration. We demonstrate its benefits against injurious processes that are interdependent and self-perpetuating [1]: a dysregulated complement system that increases with age [2], cytokine-mediated inflammation that intensifies with age [3], elevation of VEGF-A that contributes to neovascularization, and [4] oxidative stress that may injure tissues directly and induce inflammation. The inhibition of these processes was accompanied by increased cell survival and junctional integrity of RPE cells.

The inflammatory cytokines and growth factors arising from an activated complement system were suppressed in the presence of R9-SOCS3-KIR. The NF-κB promoter, which is central to the generation of inflammatory mediators, was suppressed, as shown by the blockade of the nuclear translocation of p65 and an assay of promoter activity. R9-SOCS3-KIR suppressed the expression of cytokines IL-1β, IL-6, and IL-17A and the chemokine MCP-1. IL-6 is known to compromise the eye's immune privilege [49]. Oxidative stress has been shown to increase endogenous complement-mediated responses independent of the exogenously added complement source [50]. This suggests that these two processes are interconnected and self-perpetuating. The membrane-bound receptor for C5a and C3a is present in the RPE and in several types of cells in the eye. The complement system is ordinarily part of the innate arm of the immune system, but in advanced AMD, IL-17-producing γδT cells are transported to the eye [10,50]. Thus, the adaptive immune response also participates in complement-mediated visual impairment.

The SOCS3-KIR peptide inhibits signaling downstream of the transcription factor STAT3 (Figure 7). The overactivation of STAT3 leads to elevated VEGF-A, contributing to CNV [51]. The activation of STAT3 signaling is also significant because the persistent activation of STAT3 in the retina induces visual impairment and retinal degeneration in aging mice [52]. Several groups have demonstrated the role of the SOCS3/STAT3 axis in preventing disease [18,23,24,53]. Multiple sclerosis patients on simvastatin therapy showed
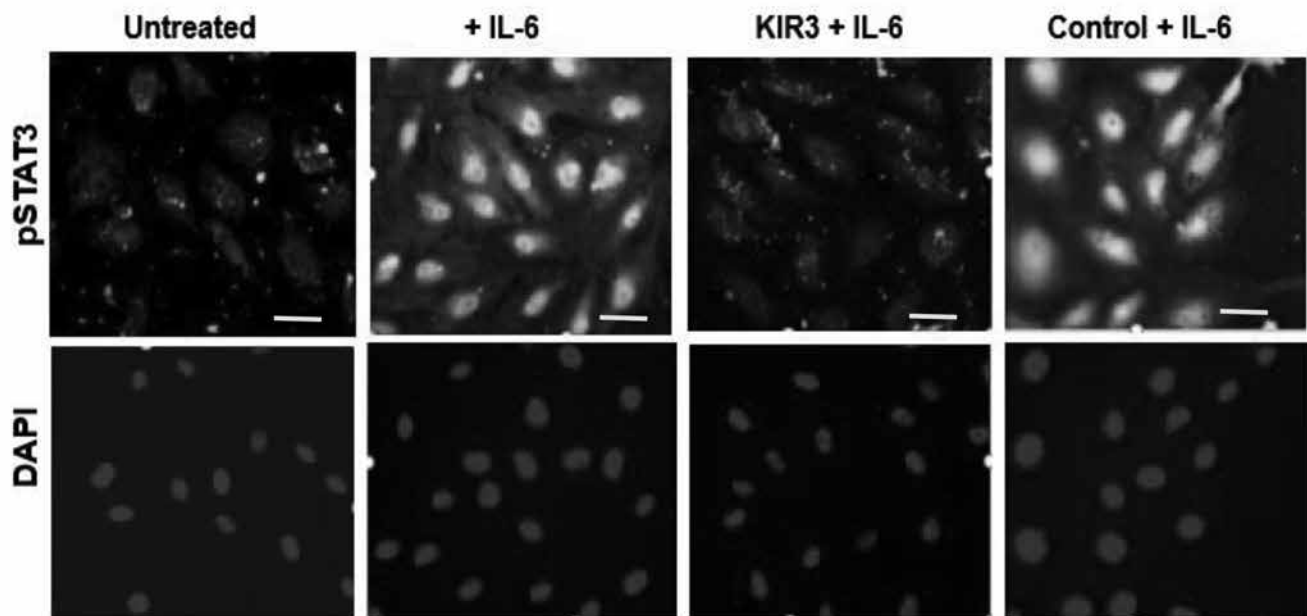

Figure 7. R9-SOCS3-KIR blocked the IL-6-mediated nuclear translocation of pSTAT3. The ARPE-19 cells in a serum-free medium were pre-treated with R9-SOCS3-KIR (20 μM) or its control peptide for 1 h and then with IL-6 (50 ng/ml) for 0.5 h. The cells were washed, stained with an antibody to pSTAT3, Alexa-488-conjugated secondary antibody, and DAPI, and then imaged using a fluorescence microscope. Scale bar: 50 μm.
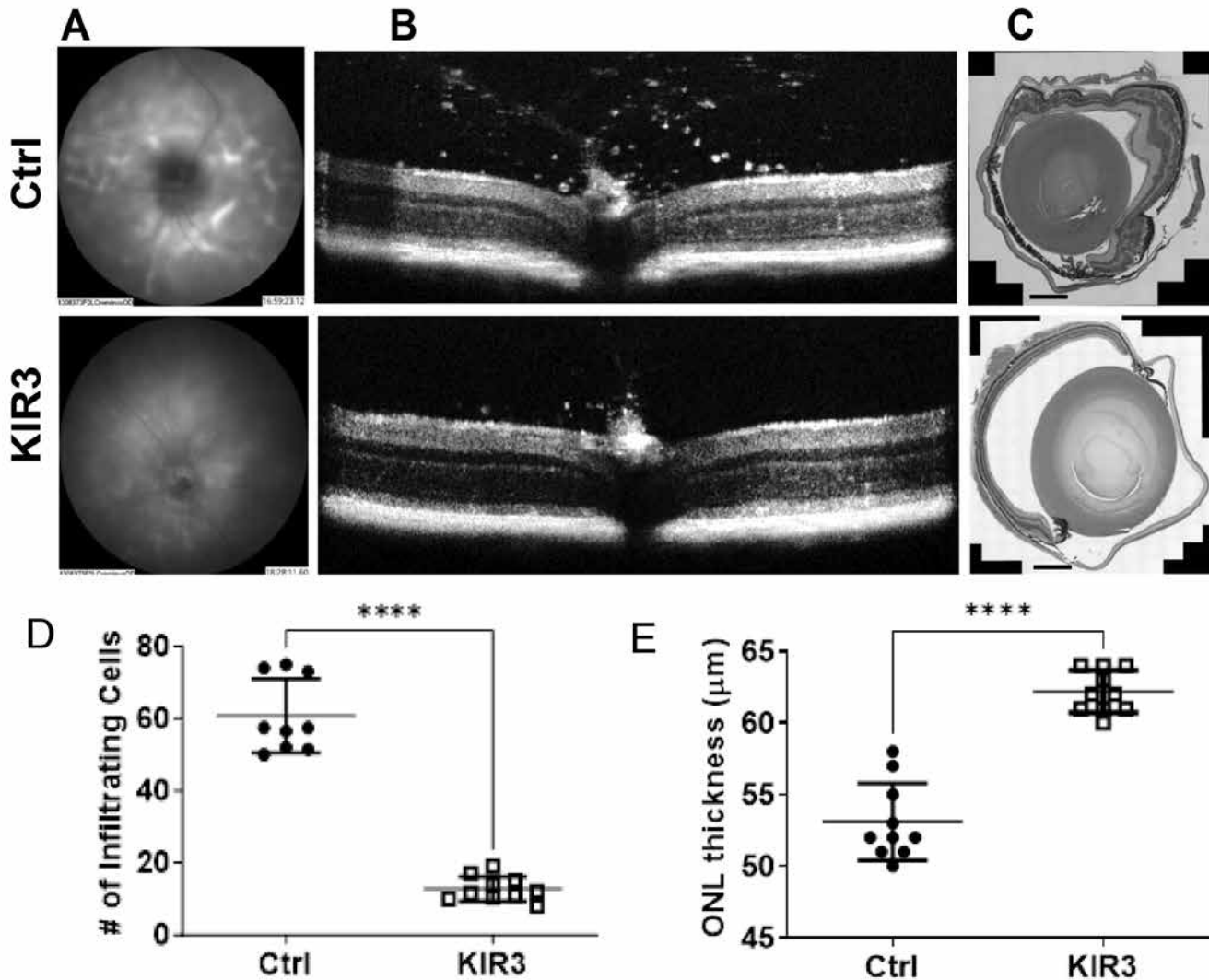
Figure 8. The corneal application of R9-SOCS3-KIR protected mouse eyes against injury caused by sodium iodate. C57BL/6 mice (10 males and 10 females) were instilled with eye drops containing R9-SOCS3-KIR or its control peptide daily (15 µg in 2 µl in each eye) one day before injecting sodium iodate (25 mg/kg) intraperitoneally. The peptides were administered daily. On day 3, fundoscopy (**A**) and spectral-domain optical coherence tomography (**B**) were performed. Hematoxylin- and eosin-stained eyes from the control and treatment eyes (**C**). Scale bar: 200 µm. The number of infiltrating cells (**D**) was counted using ImageJ. The thickness of the outer nuclear layer was measured in four different locations (temporal, nasal, superior, and inferior) at a distance of 0.35 mm from the optic nerve head using the segmentation feature of Diver 2.0 (Leica Microsystems) (**E**). The units are micrometers. Statistical significance was tested using Student's *t*-test for unpaired data. ****, $p < 0.0001$.

elevated SOCS3 levels, resulting in decreased STAT3 phosphorylation and diminished IL-6 and IL-17 levels [54,55]. Several studies have shown that SOCS3 inhibits choroidal neovascularization [56–59] and controls infection and inflammation [60,61]. Recently, the use of the KIR peptide from SOCS3, which is attached to the TAT protein domain for cell penetration, has been reported in two publications by Lu et al. to suppress IL-6 signaling in a model of traumatic brain injury [62,63]. However, the researchers used a slightly different KIR3 region than ours; we used nine arginines for cell penetration instead of the TAT peptide.

SOCS1-KIR [26,27] and SOCS3-KIR (described above) are specific and endogenous inhibitors of signaling from tyrosine kinases (e.g., JAKs and TYKs), TLR, and MAP kinases. Several tyrosine kinase inhibitors have been developed that are either monoclonal antibodies (mostly to the tyrosine kinases involved) or molecules screened from large-scale libraries with inhibitor properties. A recent example is the

use of a monoclonal antibody to treat different mutations within the myeloid–epithelial–reproductive (MER) tyrosine kinase, which causes retinitis pigmentosa of varying degrees of severity or loss of vision early in life [64]. A JAK1/JAK2 inhibitor, ruxolitinib, was therapeutic in this case. In the case of traumatic brain injury, in which MER tyrosine kinase is responsible for causing M1/M2 macrophage imbalance [65], TAM (Tyro3, Axl, and MER) activation induces the expression of SOCS1 and SOCS3, thus controlling inflammation [66].

SOCS3 deficiency in the myeloid cells of mice led to prolonged activation of the JAK/STAT pathway and elevated the expression of inflammatory cytokines, such as IL-1β, IL-6, IL-12, and IL-23 [67]. The conditional deletion of SOCS3 in blood and endothelial cells results in neutrophilia, pleural and peritoneal inflammation, and hematopoietic infiltration of several organs [68]. In the retina, photoreceptor cells express SOCS3. The conditional deletion of SOCS3 in photoreceptors suggests that it preserves the synthesis of rhodopsin, which is impaired following acute inflammation [69,70]. RPE cells also produce SOCS3 and SOCS1, and their levels are elevated in reaction to IL-17 and IFN-γ treatment, a response that can dampen an inflammatory response in the eye [71].

We demonstrate that the KIR of SOCS3 linked to a cell penetration sequence suppresses inflammatory signaling in two relevant cell types: RPE and macrophages. We also show that this peptide protects the integrity of the RPE monolayer following inflammatory insults (C5a and TNFα treatment) and protects RPE cells from mitochondrial oxidative stress induced by paraquat. The topical application of this peptide to the mouse cornea prevented injury to the retina caused by the systemic delivery of sodium iodate in a model of acute retinal/RPE oxidative stress.

We have recently reported the corneal application of R9-SOCS1-KIR to treat endotoxin-induced uveitis [27] and autoimmune uveitis as both prophylactic and therapeutic [26]. Others have developed peptide therapeutics delivered topically to limit ocular angiogenesis and provide neuroprotection [72–74]. Although considerable additional work is required to establish an appropriate dose for human eyes and to determine the pharmacokinetics of R9-SOCS3-KIR and similar peptides, it seems likely that the topical use of peptide therapeutics can be developed for clinical practice.

Abbreviations: F, Forward; R, Reverse; MCP-1, monocyte chemoattractant pretein-1; COX-2, cyclooxygenase-2; HO-1: heme oxygenase; GSTM-1: glutathione S-transferase mu 1; NQO-1: NAD(P)H dehydrogenase quinone.
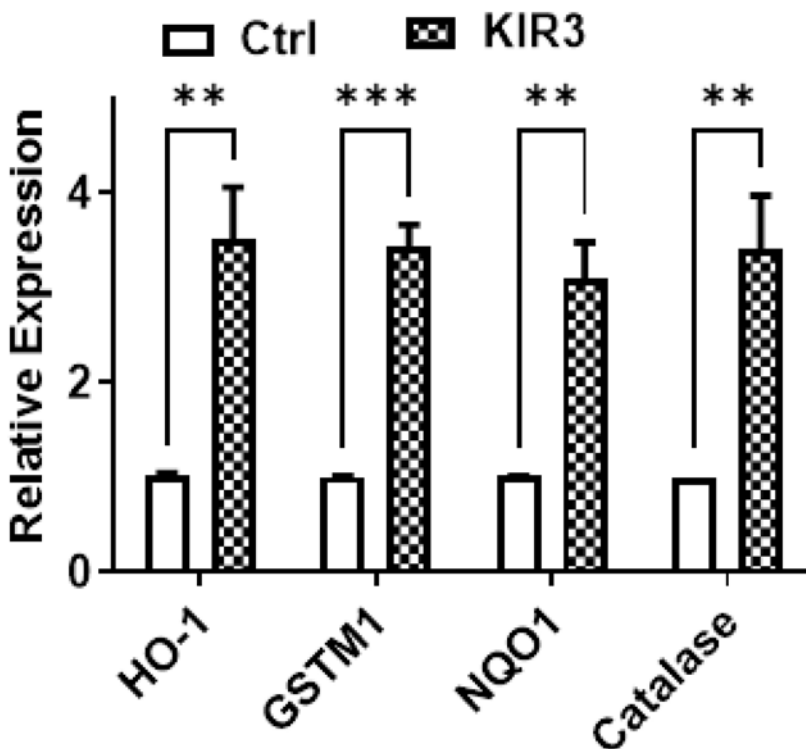

Figure 9. Eye drop instillation of SOCS3-KIR enhanced antioxidant enzymes in the retinas of mice treated with sodium iodate. Mice (n = 4 in each group) were treated on day −1 until day 3 with R9-SOCS3-KIR or the control peptide (15 µg in 2 µl in each eye) and injected i.p. on day 0 with sodium iodate. On day 3, the retina was isolated and used for RNA extraction and qRT-PCR with the target antioxidant enzymes and then compared with β-actin, which served as the internal control. In each comparison, the Student's *t*-test for unpaired data was used to establish statistical significance for each comparison. **, $p < 0.01$; ***, $p < 0.001$. Abbreviations: HO-1, heme oxygenase 1; GSTM1, glutathione S-transferase Mu 1; NQO-1, NAD(P)H quinone dehydrogenase 1.

APPENDIX 1. R9-SOCS3-KIR SUPPRESSES LPS MEDIATED INDUCTION OF NO PRODUCTION AND DECREASES INDUCTION OF IL-1B AND CYCLOXYGENASE 2.

To access the data, click or select the words "Appendix 1." **A**: Mouse macrophage cells, J774.1 were pre-treated with indicated concentrations of R9-SOCS3-KIR or the control peptide (20 μM) for 1 h, followed by addition of LPS (1 μg/ml) and the treatment overnight. Supernatants were harvested and used for NO estimation using Griess reagent. (**B**). J774A.1 cells were pre-treated with R9-SOCS3-KIR or its control peptide (20 μM) for 1 h, followed by addition of LPS (1 μg/ml) and treatment overnight. Supernatants were harvested and used for quantitation of IL-1β by ELISA. One-way ANOVA (ANOVA) followed by Tukey's test for multiple comparisons showed significant differences. **, $p < 0.01$; ***, $p < 0.001$; ****, $p < 0.0001$. (**C**) J774A.1 treated as described were lysed to obtain cell extracts. Equal amounts of proteins were separated on a polyacrylamide gel, transferred to PVDF membrane and probed with antibodies to COX-2 and α-tubulin as an internal control. (**D**) The experiment as above was repeated three times for quantitation. The relative intensities of COX-2 and α-tubulin from three different blots were measured using image J software and averaged. One-way ANOVA followed by Tukey's test for multiple comparisons showed significant differences between the treatments. **, $p < 0.01$; ****, $p < 0.0001$.

REFERENCES

1. Wong WL, Su X, Li X, Cheung CM, Klein R, Cheng CY, Wong TY. Global prevalence of age-related macular degeneration and disease burden projection for 2020 and 2040: a systematic review and meta-analysis. Lancet Glob Health 2014; 2:e106-16. [PMID: 25104651].

2. Datta S, Cano M, Ebrahimi K, Wang L, Handa JT. The impact of oxidative stress and inflammation on RPE degeneration in non-neovascular AMD. Prog Retin Eye Res 2017; 60:201-18. [PMID: 28336424].

3. Hageman GS, Luthert PJ, Victor Chong NH, Johnson LV, Anderson DH, Mullins RF. An integrated hypothesis that considers drusen as biomarkers of immune-mediated processes at the RPE-Bruch's membrane interface in aging and age-related macular degeneration. Prog Retin Eye Res 2001; 20:705-32. [PMID: 11587915].

4. Kijlstra A, Berendschot TT. Age-related macular degeneration: a complementopathy? Ophthalmic Res 2015; 54:64-73. [PMID: 26159686].

5. Ildefonso CJ, Biswal MR, Ahmed CM, Lewin AS. The NLRP3 Inflammasome and its Role in Age-Related Macular Degeneration. Adv Exp Med Biol 2016; 854:59-65. [PMID: 26427394].

6. Perez VL, Caspi RR. Immune mechanisms in inflammatory and degenerative eye disease. Trends Immunol 2015; 36:354-63. [PMID: 25981967].

7. Kauppinen A, Paterno JJ, Blasiak J, Salminen A, Kaarniranta K. Inflammation and its role in age-related macular degeneration. Cell Mol Life Sci 2016; 73:1765-86. [PMID: 26852158].

8. Khanna S, Komati R, Eichenbaum DA, Hariprasad I, Ciulla TA, Hariprasad SM. Current and upcoming anti-VEGF therapies and dosing strategies for the treatment of neovascular AMD: a comparative review. BMJ Open Ophthalmol 2019; 4:e000398 [PMID: 31909196].

9. Sharma D, Zachary I, Jia H. Mechanisms of Acquired Resistance to Anti-VEGF Therapy for Neovascular Eye Diseases. Invest Ophthalmol Vis Sci 2023; 64:28-[PMID: 37252731].

10. Coughlin B, Schnabolk G, Joseph K, Raikwar H, Kunchithapautham K, Johnson K, Moore K, Wang Y, Rohrer B. Connecting the innate and adaptive immune responses in mouse choroidal neovascularization via the anaphylatoxin C5a and γδT-cells. Sci Rep 2016; 6:23794-[PMID: 27029558].

11. Kleinman ME, Ambati J. Complement Activation and Inhibition in Retinal Diseases. Dev Ophthalmol 2016; 55:46-56. [PMID: 26501209].

12. Nozaki M, Raisler BJ, Sakurai E, Sarma JV, Barnum SR, Lambris JD, Chen Y, Zhang K, Ambati BK, Baffi JZ, Ambati J. Drusen complement components C3a and C5a promote choroidal neovascularization. Proc Natl Acad Sci U S A 2006; 103:2328-33. [PMID: 16452172].

13. Camelo S. Potential Sources and Roles of Adaptive Immunity in Age-Related Macular Degeneration: Shall We Rename AMD into Autoimmune Macular Disease? Autoimmune Dis 2014; 2014:532487[PMID: 24876950].

14. Kumar-Singh R. The role of complement membrane attack complex in dry and wet AMD - From hypothesis to clinical trials. Exp Eye Res 2019; 184:266-77. [PMID: 31082363].

15. Cao S, Wang JC, Gao J, Wong M, To E, White VA, Cui JZ, Matsubara JA. CFH Y402H polymorphism and the complement activation product C5a: effects on NF-κB activation and inflammasome gene regulation. Br J Ophthalmol 2016; 100:713-8. [PMID: 26746578].

16. Edwards AO, Ritter R 3rd, Abel KJ, Manning A, Panhuysen C, Farrer LA. Complement factor H polymorphism and

age-related macular degeneration. Science 2005; 308:421-4. [PMID: 15761121].

17. Yoshimura A, Ito M, Mise-Omata S, Ando M. SOCS: negative regulators of cytokine signaling for immune tolerance. Int Immunol 2021; 33:711-6. [PMID: 34415326].

18. Baker BJ, Akhtar LN, Benveniste EN. SOCS1 and SOCS3 in the control of CNS immunity. Trends Immunol 2009; 30:392-400. [PMID: 19643666].

19. Strebovsky J, Walker P, Lang R, Dalpke AH. Suppressor of cytokine signaling 1 (SOCS1) limits NFkappaB signaling by decreasing p65 stability within the cell nucleus. FASEB J 2011; 25:863-74. [PMID: 21084693].

20. Buchbinder EI, Desai A. CTLA-4 and PD-1 Pathways: Similarities, Differences, and Implications of Their Inhibition. Am J Clin Oncol 2016; 39:98-106. [PMID: 26558876].

21. Babon JJ, Kershaw NJ, Murphy JM, Varghese LN, Laktyushin A, Young SN, Lucet IS, Norton RS, Nicola NA. Suppression of cytokine signaling by SOCS3: characterization of the mode of inhibition and the basis of its specificity. Immunity 2012; 36:239-50. [PMID: 22342841].

22. Babon JJ, Nicola NA. The biology and mechanism of action of suppressor of cytokine signaling 3. Growth Factors 2012; 30:207-19. [PMID: 22574771].

23. Kershaw NJ, Murphy JM, Liau NP, Varghese LN, Laktyushin A, Whitlock EL, Lucet IS, Nicola NA, Babon JJ. SOCS3 binds specific receptor-JAK complexes to control cytokine signaling by direct kinase inhibition. Nat Struct Mol Biol 2013; 20:469-76. [PMID: 23454976].

24. Babon JJ, Varghese LN, Nicola NA. Inhibition of IL-6 family cytokines by SOCS3. Semin Immunol 2014; 26:13-9. [PMID: 24418198].

25. Qin H, Yeh WI, De Sarno P, Holdbrooks AT, Liu Y, Muldowney MT, Reynolds SL, Yanagisawa LL, Fox TH 3rd, Park K, Harrington LE, Raman C, Benveniste EN. Signal transducer and activator of transcription-3/suppressor of cytokine signaling-3 (STAT3/SOCS3) axis in myeloid cells regulates neuroinflammation. Proc Natl Acad Sci U S A 2012; 109:5004-9. [PMID: 22411837].

26. Ahmed CM, Massengill MT, Brown EE, Ildefonso CJ, Johnson HM, Lewin AS. A cell penetrating peptide from SOCS-1 prevents ocular damage in experimental autoimmune uveitis. Exp Eye Res 2018; 177:12-22. [PMID: 30048621].

27. Ahmed CM, Patel AP, Ildefonso CJ, Johnson HM, Lewin AS. Corneal Application of R9-SOCS1-KIR Peptide Alleviates Endotoxin-Induced Uveitis. Transl Vis Sci Technol 2021; 10:25-[PMID: 34003962].

28. Fletcher TC, DiGiandomenico A, Hawiger J. Extended anti-inflammatory action of a degradation-resistant mutant of cell-penetrating suppressor of cytokine signaling 3. J Biol Chem 2010; 285:18727-36. [PMID: 20400504].

29. Livak KJ, Schmittgen TD. Analysis of relative gene expression data using real-time quantitative PCR and the 2(-Delta Delta C(T)) Method. Methods 2001; 25:402-8. [PMID: 11846609].

30. Ildefonso CJ, Jaime H, Brown EE, Iwata RL, Ahmed CM, Massengill MT, Biswal MR, Boye SE, Hauswirth WW, Ash JD, Li Q, Lewin AS. Targeting the Nrf2 Signaling Pathway in the Retina With a Gene-Delivered Secretable and Cell-Penetrating Peptide. Invest Ophthalmol Vis Sci 2016; 57:372-86. [PMID: 26842755].

31. Luo S, Xu H, Gong X, Shen J, Chen X, Wu Z. The complement C3a-C3aR and C5a-C5aR pathways promote viability and inflammation of human retinal pigment epithelium cells by targeting NF-κB signaling. Exp Ther Med 2022; 24:493-[PMID: 35837068].

32. Yu M, Zou W, Peachey NS, McIntyre TM, Liu J. A novel role of complement in retinal degeneration. Invest Ophthalmol Vis Sci 2012; 53:7684-92. [PMID: 23074214].

33. Zhu Y, Dai B, Li Y, Peng H. C5a and toll-like receptor 4 crosstalk in retinal pigment epithelial cells. Mol Vis 2015; 21:1122-9. [PMID: 26487798].

34. Yao PL, Parmar VM, Choudhary M, Malek G. NURR1 expression regulates retinal pigment epithelial-mesenchymal transition and age-related macular degeneration phenotypes. Proc Natl Acad Sci U S A 2022; 119:e2202256119[PMID: 35867766].

35. Wang H, Han X, Wittchen ES, Hartnett ME. TNF-α mediates choroidal neovascularization by upregulating VEGF expression in RPE through ROS-dependent β-catenin activation. Mol Vis 2016; 22:116-28. [PMID: 26900328].

36. Bailey TA, Kanuga N, Romero IA, Greenwood J, Luthert PJ, Cheetham ME. Oxidative stress affects the junctional integrity of retinal pigment epithelial cells. Invest Ophthalmol Vis Sci 2004; 45:675-84. [PMID: 14744914].

37. Ablonczy Z, Dahrouj M, Tang PH, Liu Y, Sambamurti K, Marmorstein AD, Crosson CE. Human retinal pigment epithelium cells as functional models for the RPE in vivo. Invest Ophthalmol Vis Sci 2011; 52:8614-20. [PMID: 21960553].

38. Seeley JJ, Ghosh S. Molecular mechanisms of innate memory and tolerance to LPS. J Leukoc Biol 2017; 101:107-19. [PMID: 27780875].

39. Zielen S, Trischler J, Schubert R. Lipopolysaccharide challenge: immunological effects and safety in humans. Expert Rev Clin Immunol 2015; 11:409-18. [PMID: 25655761].

40. Lim LS, Mitchell P, Seddon JM, Holz FG, Wong TY. Age-related macular degeneration. Lancet 2012; 379:1728-38. [PMID: 22559899].

41. Crawford TN, Alfaro DV 3rd, Kerrison JB, Jablon EP. Diabetic retinopathy and angiogenesis. Curr Diabetes Rev 2009; 5:8-13. [PMID: 19199892].

42. Wu D, Meydani SN. Mechanism of age-associated up-regulation in macrophage PGE2 synthesis. Brain Behav Immun 2004; 18:487-94. [PMID: 15331118].

43. Terao R, Ahmed T, Suzumura A, Terasaki H. Oxidative Stress-Induced Cellular Senescence in Aging Retina and Age-Related Macular Degeneration. Antioxidants (Basel) 2022; 11:2189-[PMID: 36358561].

44. Castello PR, Drechsel DA, Patel M. Mitochondria are a major source of paraquat-induced reactive oxygen species production in the brain. J Biol Chem 2007; 282:14186-93. [PMID: 17389593].

45. Yoshimura A, Suzuki M, Sakaguchi R, Hanada T, Yasukawa H. SOCS, Inflammation, and Autoimmunity. Front Immunol 2012; 3:20-[PMID: 22566904].

46. Strebovsky J, Walker P, Dalpke AH. Suppressor of cytokine signaling proteins as regulators of innate immune signaling. Front Biosci (Landmark Ed) 2012; 17:1627-39. [PMID: 22201825].

47. Krogh Nielsen M, Subhi Y, Molbech CR, Falk MK, Nissen MH, Sørensen TL. Systemic Levels of Interleukin-6 Correlate With Progression Rate of Geographic Atrophy Secondary to Age-Related Macular Degeneration. Invest Ophthalmol Vis Sci 2019; 60:202-8. [PMID: 30644965].

48. Adamus G. Can innate and autoimmune reactivity forecast early and advance stages of age-related macular degeneration? Autoimmun Rev 2017; 16:231-6. [PMID: 28137479].

49. Ohta K, Yamagami S, Taylor AW, Streilein JW. IL-6 antagonizes TGF-beta and abolishes immune privilege in eyes with endotoxin-induced uveitis. Invest Ophthalmol Vis Sci 2000; 41:2591-9. [PMID: 10937571].

50. Liu B, Wei L, Meyerle C, Tuo J, Sen HN, Li Z, Chakrabarty S, Agron E, Chan CC, Klein ML, Chew E, Ferris F, Nussenblatt RB. Complement component C5a promotes expression of IL-22 and IL-17 from human T cells and its implication in age-related macular degeneration. J Transl Med 2011; 9:1-12. [PMID: 21762495].

51. Chen M, Lechner J, Zhao J, Toth L, Hogg R, Silvestri G, Kissenpfennig A, Chakravarthy U, Xu H. STAT3 Activation in Circulating Monocytes Contributes to Neovascular Age-Related Macular Degeneration. Curr Mol Med 2016; 16:412-23. [PMID: 27009107].

52. Marrero B, He C, Oh HM, Ukwu UT, Yu CR, Dambuza IM, Sun L, Egwuagu CE. Persistent Activation of STAT3 Pathway in the Retina Induced Vision Impairment and Retinal Degenerative Changes in Ageing Mice. Adv Exp Med Biol 2019; 1185:353-8. [PMID: 31884637].

53. Robinson GW, Pacher-Zavisin M, Zhu BM, Yoshimura A, Hennighausen L. Socs 3 modulates the activity of the transcription factor Stat3 in mammary tissue and controls alveolar homeostasis. Dev Dyn 2007; 236:654-61. [PMID: 17205581].

54. Zhang X, Jin J, Peng X, Ramgolam VS, Markovic-Plese S. Simvastatin inhibits IL-17 secretion by targeting multiple IL-17-regulatory cytokines and by inhibiting the expression of IL-17 transcription factor RORC in CD4+ lymphocytes. J Immunol 2008; 180:6988-96. [PMID: 18453621].

55. Ramgolam VS, Markovic-Plese S. Regulation of suppressors of cytokine signaling as a therapeutic approach in autoimmune diseases, with an emphasis on multiple sclerosis. J Signal Transduct 2011; 2011:635721[PMID: 22132325].

56. Stahl A, Joyal JS, Chen J, Sapieha P, Juan AM, Hatton CJ, Pei DT, Hurst CG, Seaward MR, Krah NM, Dennison RJ, Greene ER, Boscolo E, Panigrahy D, Smith LE. SOCS3 is an endogenous inhibitor of pathologic angiogenesis. Blood 2012; 120:2925-9. [PMID: 22791286].

57. Wang T, Zhou P, Xie X, Tomita Y, Cho S, Tsirukis D, Lam E, Luo HR, Sun Y. Myeloid lineage contributes to pathological choroidal neovascularization formation via SOCS3. EBioMedicine 2021; 73:103632[PMID: 34688035].

58. Sun Y, Ju M, Lin Z, Fredrick TW, Evans LP, Tian KT, Saba NJ, Morss PC, Pu WT, Chen J, Stahl A, Joyal JS, Smith LE. SOCS3 in retinal neurons and glial cells suppresses VEGF signaling to prevent pathological neovascular growth. Sci Signal 2015; 8:ra94-[PMID: 26396267].

59. Yokogami K, Yamashita S, Takeshima H. Hypoxia-induced decreases in SOCS3 increase STAT3 activation and upregulate VEGF gene expression. Brain Tumor Pathol 2013; 30:135-43. [PMID: 23104276].

60. Carow B, Rottenberg ME. SOCS3, a Major Regulator of Infection and Inflammation. Front Immunol 2014; 5:58-[PMID: 24600449].

61. Mahony R, Ahmed S, Diskin C, Stevenson NJ. SOCS3 revisited: a broad regulator of disease, now ready for therapeutic use? Cell Mol Life Sci 2016; 73:3323-36. [PMID: 27137184].

62. Cai Z, Zhang Z, Zhang L, Tan R, Wang Y, Sun M, Hu X, Ge Q, An J, Lu H. The kinase inhibitory region of SOCS3 attenuates reactive astrogliosis and astroglial scar in mice after traumatic brain injury. J Chem Neuroanat 2023; 131:102273[PMID: 37059237].

63. An J, Tan RL, Hu XX, Cai ZL, Sun MQ, Ge Q, Ma W, Li HL, Lu HX. Kinase inhibit region of SOCS3 attenuates IL6-induced proliferation and astrocytic differentiation of neural stem cells via cross talk between signaling pathways. CNS Neurosci Ther 2023; 29:168-80. [PMID: 36217678].

64. Mercau ME, Akalu YT, Mazzoni F, Gyimesi G, Alberto EJ, Kong Y, Hafler BP, Finnemann SC, Rothlin CV, Ghosh S. Inflammation of the retinal pigment epithelium drives early-onset photoreceptor degeneration in *Mertk*-associated retinitis pigmentosa. Sci Adv 2023; 9:eade9459[PMID: 36662852].

65. Wu H, Zheng J, Xu S, Fang Y, Wu Y, Zeng J, Shao A, Shi L, Lu J, Mei S, Wang X, Guo X, Wang Y, Zhao Z, Zhang J. Mer regulates microglial/macrophage M1/M2 polarization and alleviates neuroinflammation following traumatic brain injury. J Neuroinflammation 2021; 18:2-[PMID: 33402181].

66. Rothlin CV, Ghosh S, Zuniga EI, Oldstone MB, Lemke G. TAM receptors are pleiotropic inhibitors of the innate immune response. Cell 2007; 131:1124-36. [PMID: 18083102].

67. Qin H, Holdbrooks AT, Liu Y, Reynolds SL, Yanagisawa LL, Benveniste EN. SOCS3 deficiency promotes M1 macrophage polarization and inflammation. J Immunol 2012; 189:3439-48. [PMID: 22925925].

68. Ushiki T, Huntington ND, Glaser SP, Kiu H, Georgiou A, Zhang JG, Metcalf D, Nicola NA, Roberts AW, Alexander

WS. Rapid Inflammation in Mice Lacking Both SOCS1 and SOCS3 in Hematopoietic Cells. PLoS One 2016; 11:e0162111[PMID: 27583437].

69. Ozawa Y, Nakao K, Kurihara T, Shimazaki T, Shimmura S, Ishida S, Yoshimura A, Tsubota K, Okano H. Roles of STAT3/SOCS3 pathway in regulating the visual function and ubiquitin-proteasome-dependent degradation of rhodopsin during retinal inflammation. J Biol Chem 2008; 283:24561-70. [PMID: 18614536].

70. Ozawa Y, Nakao K, Shimazaki T, Shimmura S, Kurihara T, Ishida S, Yoshimura A, Tsubota K, Okano H. SOCS3 is required to temporally fine-tune photoreceptor cell differentiation. Dev Biol 2007; 303:591-600. [PMID: 17198696].

71. Ke Y, Jiang G, Sun D, Kaplan HJ, Shao H. Retinal Astrocytes respond to IL-17 differently than Retinal Pigment Epithelial cells. J Leukoc Biol 2009; 86:1377-84. [PMID: 19690291].

72. Gao W, Zhao Z, Yu G, Zhou Z, Zhou Y, Hu T, Jiang R, Zhang J. VEGI attenuates the inflammatory injury and disruption of blood-brain barrier partly by suppressing the TLR4/NF-κB signaling pathway in experimental traumatic brain injury. Brain Res 2015; 1622:230-9. [PMID: 26080076].

73. Vigneswara V, Esmaeili M, Deer L, Berry M, Logan A, Ahmed Z. Eye drop delivery of pigment epithelium-derived factor-34 promotes retinal ganglion cell neuroprotection and axon regeneration. Mol Cell Neurosci 2015; 68:212-21. [PMID: 26260110].

74. Zhang X, Li Y, Cheng Y, Tan H, Li Z, Qu Y, Mu G, Wang F. Tat PTD-endostatin: A novel anti-angiogenesis protein with ocular barrier permeability via eye-drops. Biochim Biophys Acta 2015; 1850:1140-9. [PMID: 25662072].